Response to the Referee 1's Comments

October 05, 2026

The study ***"Technical note: A decoupled in situ framework for aerosol multi-wavelength optical properties: application for lidar retrievals"*** by Yao et al. proposes a three-stage inversion for deriving lidar-relevant optical properties from ground-based in situ data. Stage 1 merges SMPS and Grimm OPC size distributions using an acceptance-angle response model and retrieves the real refractive index at 655 nm from shape consistency in the 350-750 nm overlap. Stage 2 constrains the imaginary part with AE33 absorption and propagates $n(\lambda)$ from the 655 nm anchor via a singly subtractive Kramers-Kronig relation. Stage 3 applies κ-Köhler growth and Bruggeman mixing to obtain ambient SSA and lidar ratio at 355, 532 and 1064 nm. The method is demonstrated on measurements from a 17-day campaign data over Slovenia, yielding k_{dry}=.0312/0.0238/0.0192, SSA = 0.866/0.852/0.774 and LR = 86.4/58.4/39.2 sr.

The separation of the geometric (PSD/n) problem from the absorption-constrained problem, with the dry-to-ambient conversion kept explicit, is sensible and addresses a genuine gap - boundary-layer lidar ratios, especially at 1064 nm, are poorly constrained. The manuscript is well organized and authors have commendably acknowledged several limitations about several limitations.

My main concern is that the products have not yet been shown to be quantitatively reliable. The adopted AE33 correction factor C_{eff}= 5 strongly influences the reported SSA and LR values but is not independently constrained. Moreover, the reported ± values appear to represent campaign variability rather than total retrieval uncertainty, while Monte Carlo retrieval uncertainty and structural model sensitivities are not clearly separated. Several useful checks appear possible using the existing campaign data and retrieval code.

Response: We thank the referee for the careful and constructive review. The basis and limitations of the AE33 correction assumption are addressed in Responses 1 and 2. The distinction between campaign variability, MC-propagated input uncertainty, and structural sensitivity is addressed in Response 6. Detailed responses and supporting analyses follow.

Comment 1: The manuscript does not establish an independent basis for selecting $C_{eff} = 5$ as the baseline value. Section 3.2 shows that increasing C_{eff} from 1.57 to 5 changes median SSA355 from approximately 0.684 to 0.884 and median LR_{355} from approximately 131.9 to 83.2 sr. The manuscript notes that LR_{355} at $C_{eff} = 5$ falls within a literature-guided range of approximately 60-85 sr, but later states that the literature values are used only as contextual information and not as calibration or optimization constraints. Please clearly state the decision rule used to select C_{eff}=5. The preferred options would be:

- constrained C_{eff} using an independent absorption reference, if one was available during the campaign;
- use independent scattering observations, such as a nephelometer, to evaluate the PSD-n scattering branch, while recognizing that scattering closure alone would not directly determine C_{eff};
- report the principal CRI, SSA, and LR products as a family over the tested C_{eff} range rather than presenting one value as the uniquely supported baseline. If no independent absorption or scattering reference exists, this should be stated explicitly. At minimum, the abstract should report the headline results as conditional values.

Response 1: We agree that the original manuscript did not sufficiently distinguish between a practical reference choice and an independently constrained absorption correction factor.

We have therefore revised our treatment of C_{eff}. In the revised manuscript, $C_{eff} = 5$ is no longer interpreted as an independently calibrated or uniquely supported baseline value. Instead, it is retained as a reference sensitivity scenario for presenting detailed retrieval examples and time-series/regime analyses. No independent absorption or scattering measurement was available during this campaign to determine a unique C_{eff} value. The reference value was not selected by calibration against literature LR values or used as an optimization constraint.

Accordingly, we have revised the manuscript to emphasize that the absorption-constrained CRI components and the derived SSA and LR products are conditional on the assumed C_{eff} value, whereas the step 1 PSD reconstruction and n655 retrieval are not directly determined by C_{eff}. We have also expanded the sensitivity analysis over the tested C_{eff} range (1.57–5.5) to demonstrate the influence of this assumption on the retrieved optical products.

Comment 2: Equation (3) applies a spectrally invariant C_{eff} to the complete AE33 absorption spectrum. However, all available paired reference values in Table 1 decrease with wavelength. For example, the Granada ambient values are approximately 4.72 and 3.90 at 450 and 808 nm, respectively, while the soot measurements also exhibit wavelength dependence. A constant may therefore modify the relative absorption constraints at 355, 532, and 1064 nm. This could affect the retrieved spectral ordering of k, the SSA spectrum, and the pronounced decrease of LR toward 1064 nm. Please add a sensitivity calculation

using one or more physically plausible wavelength-dependent $C_{eff}(\lambda)$ profiles based on the paired reference measurements in Table 1. The authors should report whether the following conclusions remain robust:

- $k_{355} > k_{532} > k_{1064}$
- $LR_{355} > LR_{532} > LR_{1064}$
- the relative difference among the FVF-AAE regime
- the magnitude of the reported 1064 nm LR.

The purpose for this test is not to prescribe a universal $C_{eff}(\lambda)$, but to determine whether the major spectral conclusions are sensitive to the assumption of spectrally uniform scaling.

Response 2: We evaluated the assumption of a spectrally invariant C_{eff} by repeating the retrieval using a literature-informed wavelength-dependent $C_{eff}(\lambda)$ sensitivity profile derived from the UGR-average reference values of Yus-Díez et al. (2025). The constructed profile was normalized to retain C_{355}=5, while wavelength-dependent values were obtained from interpolation and near-infrared extrapolation of the available reference spectrum (Table R1), giving C_{532}=4.36, C_{655}=4.12, and C_{1064}=4.61. Because no direct paired measurement exists at 1064 nm, this profile is used only as a physically plausible structural sensitivity scenario rather than a campaign-specific calibration.

Table R1. UGR-average reference values, normalized values, and the constructed $C_{eff}(\lambda)$ profile.

Wavelength (nm)	**370**	**450**	**470**	**520**	**590**	**660**	**808**	**880**	**950**	**1064**
UGR-average Yus-Díez et al. (2025)	4.85	4.72	4.72	4.25	4.12	3.99	3.90	3.81	4.30	
Normalized/constructed $C_{eff}(\lambda)$	5.00	4.87	4.87	4.38	4.25	4.11	4.02	3.93	4.43	4.61

Using the common paired cohort valid under both schemes (N=303), the median k spectrum retained stronger short-wavelength absorption, although the fraction of individual hours satisfying the strict $k_{355} > k_{532} > k_{1064}$ ordering was more sensitive to the assumed correction profile. In contrast, the RH-corrected LR retained the campaign-level ordering $LR_{355} > LR_{532} > LR_{1064}$, and the paired median change in LR_{1064} was approximately +0.75 sr.

The broad FVF-based LR contrasts were also preserved, whereas detailed AAE-defined subclass ordering was more sensitive and is therefore interpreted cautiously. Thus, the principal LR conclusions are stable under this tested wavelength-dependent correction, whereas detailed absorption-related spectral ordering remains conditional on the assumed $C_{eff}(\lambda)$ form. The corresponding analyses are provided in Supplement Table S5 and Fig. S3.

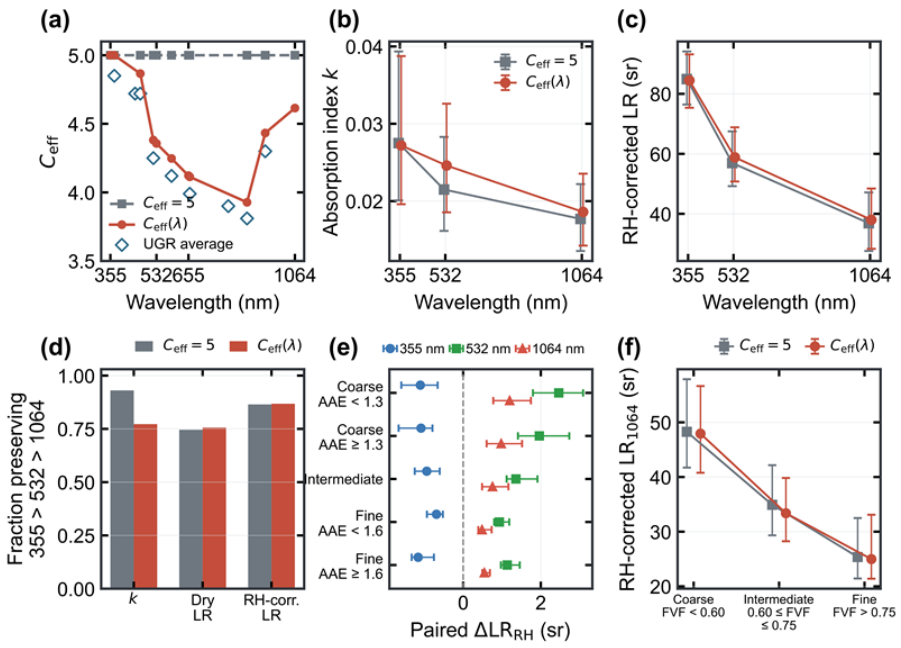

Figure R1. Sensitivity of retrieved lidar-relevant optical products to the wavelength-dependent $C_{eff}(\lambda)$ scenario. (a) Tested $C_{eff}(\lambda)$ profile relative to the scalar $C_{eff}(\lambda) = 5$ assumption. (b–c) Comparison of spectral k and RH-corrected LR under the two correction schemes. (d) Fraction of retrievals preserving the strict spectral ordering of k, dry LR, and RH-corrected LR. (e) Regime-dependent changes in RH-corrected LR. (f) Paired comparison of RH-corrected LR_{1064}. The wavelength-dependent $C_{eff}(\lambda)$ profile represents a sensitivity scenario rather than a campaign-specific calibration.

Comment 3: The synthetic forward-inverse experiment provides a useful numerical closure test, but the manuscript correctly acknowledges that it is not independent validation because the synthetic truth and retrieval use the same physical model and assumptions. Given the lidar-oriented framing, the availability of collocated or nearby lidar and sun-photometer observations during 7-23 April 2016 should be stated explicitly. The manuscript cites previous lidar work in the Vipava Valley environment, but it is unclear whether vertically resolved observations were available during the campaign period. If temporally collocated lidar measurements exist, please compare the RH-corrected 532 nm extinction or LR with the lowest range bins for which overlap correction is reliable. Such a comparison should be restricted to periods when the lower boundary layer can reasonably be considered vertically well mixed. If sun-photometer observations are available, comparison with AOD would require a defensible vertical integration of the locally derived extinction coefficient, for example using a lidar extinction profile or independently determined boundary-layer height. If neither lidar nor sun-photometer observations are available, this should be stated clearly in Section 2.1, and the abstract and conclusions should more explicitly describe the results as internally consistent, site-specific, ambient-equivalent estimates rather than independently validated lidar products.

Response 3: We agree that the synthetic forward–inverse experiment should be regarded as a numerical closure test rather than an independent validation, because the synthetic observations and the retrieval share the same forward-model assumptions.

A single-wavelength elastic lidar operating at 1064 nm was available during the 7–23 April 2016 campaign period. However, its aerosol backscatter profiles were retrieved using a Klett-type elastic-lidar inversion, which requires an assumed lidar-ratio constraint and retrieval boundary conditions. Therefore, the lidar observations do not provide an independent extinction coefficient or an independent lidar-ratio constraint for validating the present retrieval.

No suitable temporally collocated sun-photometer AOD dataset was available for the campaign period. Moreover, an AOD comparison would require an independently constrained vertical extinction profile, which is unavailable for this dataset.

We have therefore revised the manuscript to clarify that the reported quantities represent internally consistent, site-specific, near-surface ambient-equivalent aerosol optical estimates under the adopted assumptions rather than independently validated lidar products. Their application as lidar-relevant constraints should therefore be interpreted primarily for near-surface or vertically well-mixed lower-boundary-layer conditions.

Comment 4.1: The reconstructed PSD underpins the retrieval of n_{655}, extinction, backscatter, SSA, and LR. The coarse tail may exert disproportionate control over the 1064 nm backscatter and therefore the reported LR_{1064}.The manuscript shows $PM_{2.5}$ and PM_{10}, but it does not explain how these quantities were measured or derived. Please identify the instruments or procedures used to obtain PM data. If PM was measured independently of the Grimm OPC, integration of the reconstructed PSD using plausible mode-dependent densities could provide a valuable mass-closure test. Such a comparison should account for:

- whether the PSD and PM measurements represent dry or ambient aerosol;
- density and dynamic shape factor;
- the instrument inlet and transmission efficiency;

If the PM concentrations were themselves derived from the Grimm OPC, they should not be described as an independent validation of the reconstructed PSD.

Response 4.1: We thank the reviewer for requesting clarification of the PM quantities. The $PM_{2.5}$ and PM_{10} values shown in the manuscript were not obtained from an independent gravimetric or regulatory mass instrument. They were derived from the reconstructed SMPS–OPC number-size distribution and are therefore described as PSD-derived mass-equivalent diagnostics, not as independent validation of the reconstructed PSD. The reconstructed PSD was converted to a mass distribution using prescribed densities of 1.8 g cm^{-3} for $D_g \leq 1$ μm and 2.62 g cm^{-3} for $D_g > 1$ μm. A dynamic shape factor $\chi = 1$ and reference density ρ_0 =1 g cm^{-3} were assumed. Geometric-equivalent diameter was approximately mapped to aerodynamic-

equivalent diameter and the resulting mass distribution was integrated below 2.5 and 10 μm, with fractional treatment of bins intersecting the cutoff.

We have revised the Methods and relevant figure discussion to clarify that the reported $PM_{2.5}$ and PM_{10} values represent internal mass-equivalent diagnostics derived from the reconstructed PSD and should not be interpreted as independent validation of the size reconstruction.

Table R2. Assumptions used for PSD-derived $PM_{2.5}$ and PM_{10} mass-equivalent diagnostics.

Parameter	Value
Density fine mode	1.8 g cm^{-3}
Density coarse mode	2.62 g cm^{-3}
Shape factor	1
Reference density	1 g cm^{-3}
Integration method	size-bin integration

Comment 4.2: Similarly, the eBC series in Figure 8 appears to be derived using the same AE33 observations and the adopted C_{eff} = 5. It therefore cannot independently constrain C_{eff} unless an external refractory-BC or absorption reference was used. Please explain how eBC was calculated, including the assumed MAC and its wavelength dependence.

Response 4.2: We thank the reviewer for raising this important point. The eBC series used in the regime analysis (Supplement Fig. S6a) was not used as an independent constraint for determining C_{eff}. No independent refractory-BC measurement or external calibration reference was available during this campaign. Therefore, eBC is used only as an AE33-derived diagnostic indicator of absorbing-aerosol loading, rather than as an independent validation dataset for selecting C_{eff}. The plotted eBC is derived from the same AE33 absorption measurement used in the optical retrieval.

Specifically, the eBC was calculated from the AE33 absorption at 880 nm after applying the adopted C_{eff} = 5 correction:

$$eBC_{880}^{C_{eff}} = \frac{C_{default}}{C_{eff}} \frac{\alpha_{abs,880}^{C_{default}}}{MAC_{880}}$$

with $C_{default}$=1.57 and MAC_{880}=7.77 m^2 g^{-1}. We have revised the manuscript to describe it as an AE33-derived absorbing-aerosol loading diagnostic under the adopted C_{eff}, rather than as an independent validation of C_{eff}.

Comment 4.3: The inlet configuration, sampling-line length, flow conditions, and effective upper-size transmission should also be reported. Without this information, it is difficult to assess whether the reported PSD extending to 20 μm, particularly the portion above approximately 5-10 μm, is quantitatively representative.

Response 4.3: We have expanded the description of the sampling configuration and operating flow conditions. The fine-mode PSD was measured with a GRIMM SMPS+C system equipped with a long differential mobility analyzer (L-DMA), operated at the standard aerosol and sheath flow settings of 0.3 and 3.0 L min^{-1}, respectively. The GRIMM 1.109 OPC sampled through a TSP-type inlet at its nominal flow rate of 1.2 L min^{-1}, while the AE33 used a separate $PM_{2.5}$ inlet at 5 L min^{-1}. An available raw AE33 file from the same deployment records a median total flow of 5 L min^{-1}, consistent with this operating setting. The sampling line was approximately 3 m long, used nominal 6.35 mm tubing. The SMPS, OPC and AE33 used separate sampling lines.

For context, Lill et al. (2024) used the same GRIMM 1.109 at the same flow rate with an approximately 1.5-m vertical 6.35 mm line and estimated transmission of approximately 99–88% over 0.25–10 µm. Zinke et al. (2024) similarly operated a GRIMM 1.109 through a 5-m vertically downward 6.35 mm line with a 180° bend and explicitly evaluated diffusion, impaction, and sedimentation losses, which contributed only approximately 0.6–1.5% across their analysed 0.25–2.5 µm size range. We use these results only as configuration-based benchmarks rather than transferring their transmission efficiencies directly to Vipava. The potential influence of the upper coarse-particle range on the retrieved optical properties is further evaluated through the truncation sensitivity tests described in Response 5.1.

Comment 4.4: Additionally, the synthetic test indicates that the real refractive index is less robustly recovered than the imaginary part and remains sensitive to PSD remapping and OPC-response assumptions. Please provide an objective measure of SMPS-OPC overlap quality and examine the sensitivity of to the selected overlap interval and plausible relative SMPS-OPC concentration offsets. The authors should also state whether retrievals with poor overlap or weakly constrained solutions were rejected. This would help demonstrate that the retrieved rather than only the smoothness of the merged PSD, is adequately constrained.

Response 4.4: We thank the reviewer for requesting a more explicit assessment of SMPS–OPC overlap consistency and real-refractive-index identifiability. We therefore provide an overlap-based objective-profile analysis and structural sensitivity tests for n_{655} below (Fig. R3). The corresponding diagnostic definitions and QA/QC treatment have also been added to Supplement Sect. S2 and Table S3.

We treated retrieval screening separately from overlap and identifiability diagnostics. A minimum loading criterion of $PM_{1,\,ref} \geq 3$ µg m^{-3} was applied, following the minimum aerosol loading above which Di Antonio et al. (2025) found size-distribution and refractive-index retrievals to remain well constrained. In addition, we introduced a post-retrieval lower-RRI plausibility criterion of $n_{655} \geq 1.33$, corresponding to the lower bound (n=1.33) of the retrieved real refractive index in the AERONET inversion framework (Sinyuk et al., 2020). We use 1.33 here as an operational, literature-informed lower plausibility limit rather than as a universal

physical bound. Five otherwise retained retrievals with $n_{655} < 1.33$ were excluded, yielding a final cohort of N=304.

The identifiability of the retrieved real refractive index was further assessed using the objective-function profile $J(n)$ over the LUT range $1.30 \le n \le 1.70$ (Fig. R3a). For each candidate n, the remaining fitted parameters were re-optimized. The normalized objective profile and the descriptive relative-5 % profile-wide support width were defined as

$$\tilde{J}(n) = \frac{J(n) - J_{\min}}{J_{\max} - J_{\min}}, \quad W_{5\%} = \max_{\tilde{J}(n) \le 0.05} n - \min_{\tilde{J}(n) \le 0.05} n, \quad 1.30 \le n \le 1.70.$$

Here, $J_{\min}$ and $J_{\max}$ denote the minimum and maximum objective values over the evaluated LUT range, respectively. A smaller $W_{5\%}$ indicates that the overlap information constrains n more tightly. $W_{5\%}$ is a descriptive identifiability diagnostic rather than a statistical confidence interval. When the selected support contained disconnected components, $W_{5\%}$ represented their overall profile-wide span, while the individual components were retained in Fig. R3a.

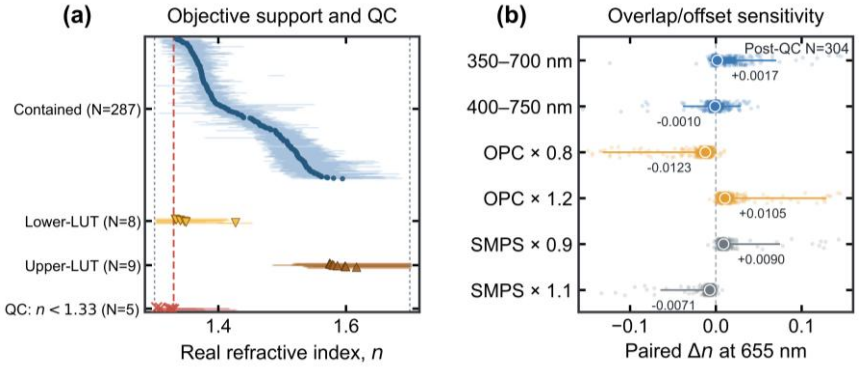

Figure R3. (a) Descriptive 5%-of-profile-range supports (light lines) and best-fit n (symbols) for the 309 hard-valid candidates; red dashed: n_{655} = 1.33 screen. (b) Paired Δn_{655} (N = 304) under overlap-window and concentration-offset perturbations; circles: medians; bars: IQR and P2.5–P97.5.

The structural sensitivity of the retrieved n_{655} was quantified by repeating the retrieval with alternative overlap intervals of 350–700 and 400–750 nm and with relative concentration perturbations of OPC ×0.8/1.2 and SMPS ×0.9/1.1. For the final N=304 retrievals, the median paired changes in n_{655} were +0.0017 and −0.0010 for the two overlap-window tests, −0.0123 and +0.0105 for OPC ×0.8 and ×1.2, and +0.0090 and −0.0071 for SMPS ×0.9 and ×1.1, respectively (Fig. R3b).

Comment 5.1: The reported mean LR_{1064} = 39.2 sr depends on several weakly constrained elements: the coarse-mode PSD retrieved from a single-wavelength OPC through an assumed response model, extrapolation of the AE33 absorption fit beyond its longest measurement wavelength, SSKK propagation furthest from the 655 nm anchor, and spherical Mie calculations in an environment affected by episodic coarse-mode and dust

enhancement. Please add PSD-truncation tests by recalculating the optical products with upper-diameter cut-offs of 2.5, 5, and 10 µm. Cumulative size-resolved contributions to extinction and backscatter at 355, 532, and 1064 nm would further clarify which particle sizes control the reported LR spectrum.

Response 5.1: We evaluated the sensitivity of the retrieved optical products to the uncertain coarse-particle size range by recalculating the RH-corrected optical properties after truncating the dry reconstructed PSD at D_{max}=2.5, 5, and 10 µm, using the full PSD extending to approximately 20 µm as the reference. For each cutoff, the retrieved refractive index, RH, hygroscopicity parameters, and wet-state mixing treatment were unchanged, and concentrations below the cutoff were not renormalized.

The revised post-QC cohort (N=304) gives a campaign-mean RH-corrected LR_{1064} of 39.81 sr updated from 39.2 sr in the original manuscript. The magnitude of the PSD-truncation response increases markedly toward 1064 nm (Fig. R4 a, b). Importantly, truncating the coarse tail decreases rather than increases LR_{1064}, while the campaign-level ordering $LR_{355} > LR_{532} > LR_{1064}$ remains unchanged under all three cutoff tests. Thus, the coarse-size extension affects the absolute magnitude of LR_{1064}, but does not produce its relatively low value.

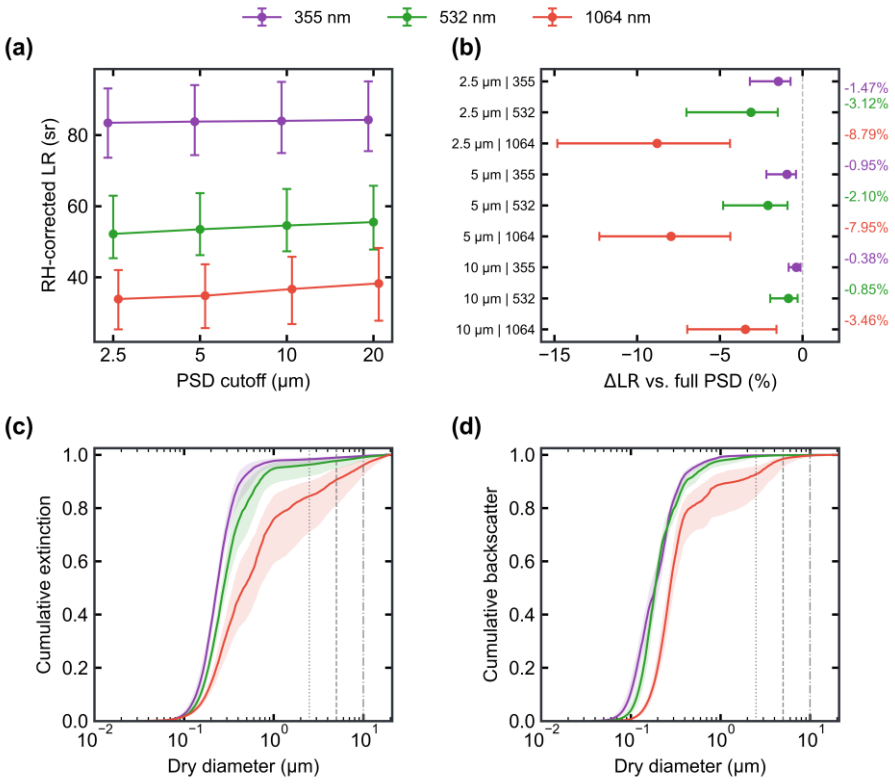

Figure R4. Sensitivity of RH-corrected optical properties to truncating the dry reconstructed PSD at upper cut-offs of D_{max} = 2.5, 5, and 10 µm, referenced to the full PSD extending to 20 µm (post-QC cohort, N = 304).

Table R3. Median RH-corrected lidar ratios and median paired hourly relative changes under PSD upper-diameter truncation.

D_{max}	Median LR_{1064} (sr)	ΔLR_{355}	ΔLR_{532}	ΔLR_{1064}
2.5 μm	33.88	−1.47%	−3.12%	−8.79%
5 μm	34.80	−0.95%	−2.10%	−7.95%
10 μm	36.69	−0.38%	−0.85%	−3.46%
20 μm	38.27	Reference	Reference	Reference

The cumulative size-resolved calculations in Figure R4(c, d) explain this behaviour. At 1064 nm, particles below 2.5, 5, and 10 μm contributed 84.48%, 90.60%, and 96.10% of extinction, respectively, compared with 92.78%, 98.45%, and 99.69% of backscatter. The coarse-size contribution is therefore proportionally larger for extinction than for backscatter at 1064 nm; removing progressively more of the coarse tail decreases extinction more strongly than backscatter and consequently lowers LR_{1064}.

Thus, coarse-size support affects the absolute LR_{1064} magnitude, primarily through the 2.5–10 μm range, but does not produce the low LR_{1064} value or alter the campaign-level spectral ordering. The PSD-cutoff tests quantify this structural sensitivity and are not used as a retrospective correction of the OPC sampling transmission.

Comment 5.2: Particle nonsphericity should also be discussed explicitly, because nonspherical coarse particles may produce substantially different backscatter from equivalent spheres and could contribute to uncertainty in the low reported LR_{1064}. This is particularly relevant to the contrast with Haarig et al. (2018) discussed in Section 4.2.

Response 5.2: We have revised the discussion to address particle nonsphericity as a potential model-form uncertainty in the lidar ratio. Particle shape can strongly affect 180° backscatter, and previous modelling and measurement studies have demonstrated that smoke backscattering depends on particle morphology, size distribution, and refractive index (Liu and Mishchenko, 2020; Gialitaki et al., 2020; Qin et al., 2024; Huang et al., 2023).

For the revised N=304 cohort, particles larger than 2.5 μm accounted for 15.52% of the modelled extinction and 7.22% of the modelled backscatter at 1064 nm. Removing this size range changed the median LR_{1064} from 38.27 to 33.88 sr, while the median paired relative change was −8.79%. Thus, within the spherical-Mie calculation, the coarse tail increases LR_{1064}. If irregular coarse particles produce weaker 180° backscatter than equivalent spheres while extinction is less affected, the spherical calculation would underestimate LR_{1064}. However, because hour-resolved quantitative shape constraints and collocated depolarization measurements are unavailable, this effect cannot be quantified. Particle nonsphericity may therefore contribute to the difference from the values reported by Haarig et al. (2018). Differences in aerosol population, size distribution, refractive index, absorption, and sampling context may also contribute.

Comment 5.3: Finally, the coarse-influenced regime has a higher median LR_{355} than the fine-mode-dominated regime, 88.4 versus 79.8 sr. Please explain this behaviour, preferably by decomposing extinction and backscatter contributions from the fine and coarse modes.

Response 5.3: We performed an additional fine/coarse-mode decomposition of the RH-corrected 355 nm extinction and backscatter, using D_p=1 μm as the mode boundary. Following the revised post-retrieval QC, the median LR_{355} is 89.87 sr for the coarse-influenced group (FVF < 0.60, N = 115) and 78.31 sr for the fine-dominated group (FVF > 0.75, N = 86).

In the coarse-influenced group, coarse particles accounted for median contributions of 6.05% to extinction and 1.28% to backscatter at 355 nm, compared with 0.93% and 0.63%, respectively, in the fine-dominated group (Fig. R5). Because the coarse-mode contribution was proportionally greater for extinction than for backscatter, including this mode increased LR_{355}. The median paired increase relative to the fine-mode-only calculation was +3.42 sr in the coarse-influenced group and +0.30 sr in the fine-dominated group.

The coarse mode did not, however, explain the full inter-group difference: the median fine-mode-only LR_{355} was already 85.40 sr in the coarse-influenced group and 77.77 sr in the fine-dominated group. The higher total LR_{355} therefore reflects both the difference in fine-mode optical response between the two groups and the larger extinction-dominant coarse-mode contribution in the coarse-influenced group.

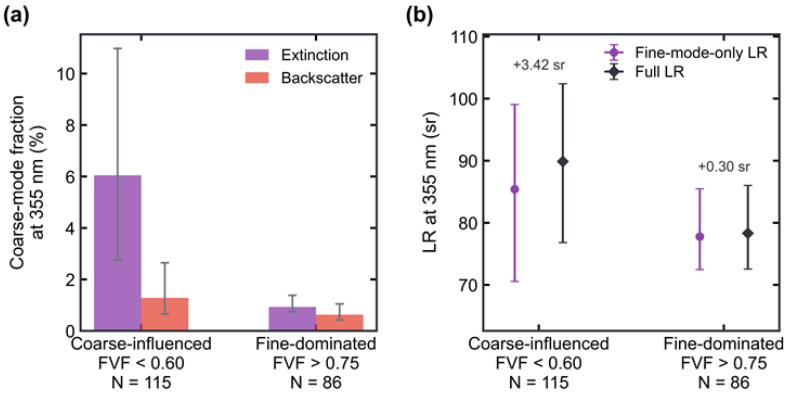

Figure R5. Fine/coarse mode decomposition of the 355 nm RH-corrected lidar ratio difference between FVF regimes. (a) Relative coarse-mode contributions to extinction and backscatter. (b) Comparison between fine-mode-only and full LR355, showing the contribution of coarse-mode inclusion.

Comment 6: No perturbation magnitudes, probability distributions, or correlation structures are provided for the 500-realisation Monte Carlo analysis (L167–169). Please report these assumptions for each instrument. The meaning of the reported ± values should also be clarified. For example, LR_{355} = 86.4 ± 12.7 sr appears to represent the campaign mean ± standard deviation rather than total retrieval uncertainty. Please distinguish among

campaign temporal variability, Monte Carlo retrieval uncertainty, and structural sensitivity, including C_{eff}, the OPC response assumption, prescribed hygroscopicity parameters, particle sphericity, and the homogeneous-equivalent assumption. A short table separating these terms would substantially improve the usability of the products. Regarding the identical ± 0.075 values reported for n_{dry} at all three wavelengths represent campaign variability, Monte Carlo uncertainty, propagation from the common 655 nm anchor, or rounding.

Response 6: We thank the reviewer for identifying this ambiguity. We added Sect. 2.3 and main-text Table 1 to distinguish campaign temporal variability, MC-propagated measurement-input uncertainty, deterministic structural sensitivity, and fixed/model-form assumptions. The full perturbation distributions and correlation structure are provided in Supplement Sect. S3 and Table S4.

For each retained hourly retrieval, 500 MC realizations were run using multiplicative mean-one lognormal perturbations with relative standard deviations of 10%, 20%, and 20% for the SMPS number concentrations, OPC number concentrations, and AE33 absorption inputs, respectively. SMPS bins and OPC channels were perturbed independently, AE33 perturbations were independent among wavelengths, and the instrument groups were mutually independent. MC summaries were calculated from realizations satisfying the predefined retrieval-validity criteria.

The MC ensemble quantifies propagation of the prescribed measurement-input perturbations, not total retrieval uncertainty. Structural choices were evaluated separately through deterministic sensitivity tests, while prescribed hygroscopicity, spherical-particle optics, and homogeneous-equivalent mixing remain fixed/model-form limitations (Table R4).

The reviewer's interpretation of the originally reported "±" values is correct. The original LR_{355} = 86.4 ± 12.7 sr represented the campaign mean ± between-hour SD, rather than MC or total retrieval uncertainty. The originally reported n_{dry} standard deviations likewise represented between-hour variability and all rounded to 0.075. The revised post-QC N = 304 results are 1.449 ± 0.076, 1.441 ± 0.075, and 1.437 ± 0.075 at 355, 532, and 1064 nm, respectively, with "±" explicitly defined as the between-hour SD.

Table R4. Separation of campaign variability, Monte Carlo input uncertainty, structural sensitivity, and fixed/model-form assumptions.

Category	Treatment	Interpretation / Reporting
Campaign temporal variability	Across-hour statistics for the post-QC cohort (N = 304)	Mean ± SD and percentiles describe temporal variability, not retrieval uncertainty
MC-propagated input uncertainty	500 mean-one lognormal realizations per retained hour: SMPS 10%, OPC 20%, and AE33 20% relative SD	MC SD and P2.5–P97.5 from valid realizations quantify input-propagation spread only

Category	Treatment	Interpretation / Reporting
Deterministic structural sensitivity	Alternative $C_{eff}/C_{eff}(\lambda)$, overlap/remapping, concentration-offset, PSD-cutoff, and RH-treatment scenarios	Paired scenario-dependent changes; not confidence intervals
Fixed/model-form assumptions	Prescribed $\kappa_f = 0.2$ and $\kappa_c = 0.03$ were not sampled; spherical Mie; Bruggeman equivalent-medium treatment	Not probabilistically sampled; no total uncertainty estimate

Comment 7.1: Lines 347-355 present a detailed diurnal source interpretation involving 6 a.m. traffic and charcoal combustion, industrial emissions at noon, and nitrate/sulfate dominance, but no composition data or supporting citations are provided. Please support these claims or reduce the passage to what the optical data show. If SEM or mineralogical analyses of campaign filter samples exist, they could substantiate the dust interpretation. For example, the early-morning increase in k may be described as evidence of enhanced short-wavelength absorption without assigning a unique emission source.

Response 7.1: We thank the reviewer for this important comment. We agree that the original discussion assigned specific emission sources and chemical components to the diurnal optical variations beyond what was supported by temporally matched measurements. In particular, the previous attributions to early-morning traffic and charcoal combustion, daytime industrial emissions, nitrate/sulfate dominance, and the evening coexistence of traffic, industrial, and residential emissions were not directly constrained by the measurements used in the present retrieval. These source-specific statements have therefore been removed.

The revised interpretation of Figure 7 is restricted to the optical behaviour directly supported by the observations. The early-morning increase in k_{dry} at approximately 05:00–07:00 LST is now described as enhanced short-wavelength absorption, with k_{355} generally exceeding k_{532} and k_{1064}, without assigning a unique emission source. The associated variations in RH-corrected SSA and LR are likewise discussed as wavelength-dependent optical responses rather than as source- or composition-specific signatures.

Following the reviewer's suggestion, we have also incorporated the available SEM–EDX evidence from filter samples collected during the same April 2016 Vipava Valley campaign. It provides qualitative evidence for mineral-containing particles during a dust-influenced episode, but is not temporally resolved to the hourly composite and is therefore used only as campaign-level context.

To retain the relevant regional context without reintroducing unsupported source attribution, we have further cited previous observations from the Vipava Valley and the northern Adriatic region. Subsequent lidar observations in the Vipava Valley identified aerosol states consistent

with mixtures of combustion-related aerosol, mineral dust, and marine aerosol under different transport and meteorological conditions (Wang et al., 2022). Regional chemical measurements have also reported sulfate-, ammonium-, and nitrate-containing fine aerosol and sea-salt-related components in the Slovenian and northern Adriatic coastal environment (Turšič et al., 2006; Gluščić et al., 2020). These studies establish the potential complexity of the regional aerosol population but do not determine the composition of the individual hourly samples analysed here.

Comment 7.2: Separately, Section 2.1 lists only the SMPS, OPC, and AE33, whereas the results also use $PM_{2.5}$, PM_{10}, and station RH. Please describe these additional measurements and explain the visible data gaps in Figure 6, around 13-15 and 17-19 April, with valid-sample counts.

Response 7.2: We have revised Sect. 2.1 and the Fig. 6 caption to clarify the provenance of $PM_{2.5}$, PM_{10}, and station RH. $PM_{2.5}$ and PM_{10} were not independently measured, but were derived from the reconstructed dry SMPS–OPC PSD using aerodynamic-equivalent cutoffs and prescribed fine/coarse densities of 1.8 and 2.62 g cm−3, respectively. Station RH observations from the local meteorological station in Ajdovščina were averaged to hourly resolution and used as the ambient-RH input.

The revised Fig. 6 is plotted on the fixed analysis window from 7 April 00:00 to 23 April 00:00 (385 hourly timestamps). Across input screening and retrieval-validity checks, 76 timestamps were excluded: 27 were absent from the aligned source record, 15 had all-null AE33 data, 1 failed numerical retrieval validity, 26 were precipitation-screened, and 7 otherwise valid hours were below the minimum-loading applicability criterion. This yielded 309 hard-valid retrieval candidates. A further five candidates with $n_{655} < 1.33$ were excluded by the post-retrieval plausibility screen, producing the final post-QC cohort of N=304 used for the reported optical statistics. The minimum-loading screen uses the separate SMPS-derived metric $PM_{1,\,ref}$ ($D \leq 1$ µm; 1.4 g cm^{-3}) and is distinct from the PSD-derived PM2.5 and PM10 diagnostics.

The main visible gaps arise from missing AE33 absorption on 13 April 08:00–22:00 and complete measurement unavailability from 17 April 04:00 to 18 April 06:00; shorter gaps are mainly precipitation-screened periods.

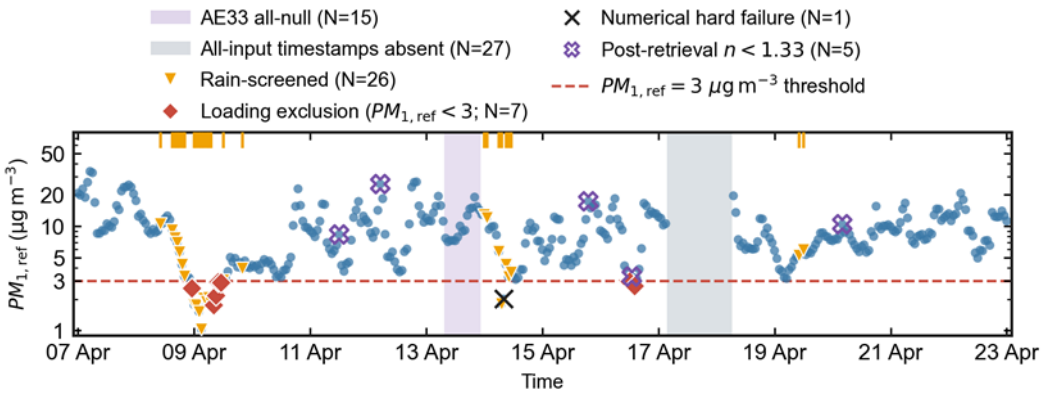

Figure R6. Hourly $PM_{1,ref}$ over the 7–23 April 2016 analysis window (385 hours)

Comment 8: Text says outputs at 355, 532, 655 and 1064 nm; results show three wavelengths only.

Response 8: We thank the reviewer for identifying this inconsistency. The 655-nm wavelength is not a final optical-output wavelength in this study. It corresponds to the OPC optical wavelength and is used as the anchor for retrieving n_{655} from the SMPS–OPC overlap. The final lidar-oriented optical products are calculated at 355, 532, and 1064 nm. We have revised the manuscript to distinguish the intermediate 655-nm OPC anchor from the three reported lidar wavelengths.

Comment 9: Eq. (1), Line 143 - 'x' is undefined (presumably size parameter); λ is defined but does not appear. Please define all symbols and state the normalisation of $w_{optics}(\theta)$.

Response 9: Thank you for pointing this out. We have revised Eq. (1) and the accompanying text to define $x = \pi D_p/\lambda$, where D_p is the particle diameter and λ = 655 nm is the OPC laser wavelength. We also clarified the angular weighting used in the OPC response calculation. Following the OPC response treatment of Heim et al. (2008), $w_{optics}(\theta)$ is defined as a dimensionless relative angular-response weighting, with a value of 2.0 over 81°–98° and 1.0 over the remainder of the 30°–150° integration interval. No additional normalization to unit integral or unit mean is applied. Since the same weighting convention is used for both calibration-particle and aerosol-particle responses, any common multiplicative normalization factor cancels in the response ratio used for OPC diameter mapping.

Comment 10: Please state how many samples fall in the RH < 40 %, 40-95 % and >95 % bins, and confirm no artificial step appears near RH = 40 % in Fig. 12c.

Response 10: We thank the reviewer for raising this important point regarding the implementation of the RH correction and the potential influence of the selected 40% RH

reference condition. Of the 304 post-QC hours, 29 fall in the RH < 40% reference state, 260 in the 40–95% hygroscopic-growth range, and 15 were capped at 95% RH.

In the revised manuscript, we clarified that the 40% RH value is used as an operational low-RH reference state rather than a physical threshold for aerosol phase transition. Because the SMPS–OPC measurements represent a low-RH operational reference state rather than an ideal completely dry aerosol state, we do not interpret observations below 40% RH as an ideal dry state. Instead, no additional hygroscopic water uptake is applied relative to this reference condition, and the growth factor is defined as $GF_{s,rel}$ =1 for RH < 40%.

For RH ≥ 40 %, the hygroscopic growth factor is calculated relative to this reference condition using the normalized formulation:

$$GF_{s,rel} = \frac{\left[1+\kappa_s RH/(100-RH)\right]^{1/3}}{\left[1+\kappa_s RH_{ref}/(100-RH_{ref})\right]^{1/3}}$$

where RH_{ref}= 40%. Therefore, the calculated growth factor satisfies $GF_{s,rel}$ = 1 at the reference RH, providing a continuous transition between the low-RH reference state and the RH-dependent growth regime.

As shown in Fig. R7(a), the calculated growth factor is continuous at RH=40% for both fine and coarse modes. Furthermore, the RH-induced optical response does not show an abrupt change at the transition point (Fig. R7(b)). Within the 38–40% RH interval, the paired lidar-ratio changes remain zero because these observations follow the defined reference-state treatment. Immediately above the reference condition (40–42% RH), only small gradual changes are observed (+0.063 sr, −0.025 sr, and −0.190 sr for 355, 532, and 1064 nm, respectively), indicating a progressive RH response rather than a discontinuous jump.

We have revised Section 2.2.5 to clarify that the 40% RH value represents an operational reference condition for calculating additional hygroscopic effects. This treatment avoids introducing an artificial discontinuity while allowing the RH-corrected optical properties to represent changes relative to the observed low-RH aerosol state.

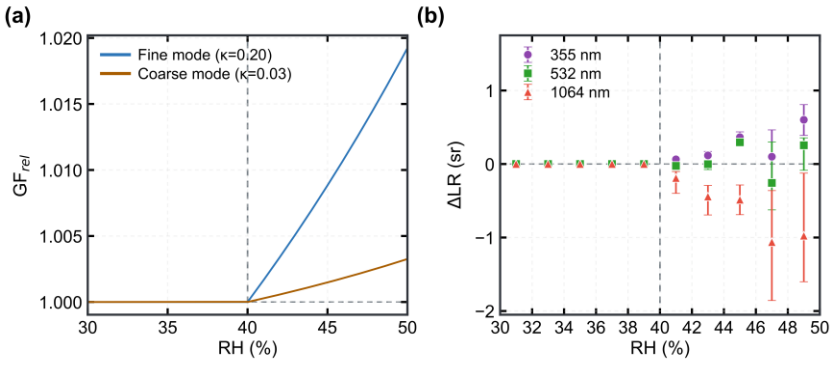

Figure R7. Operational RH treatment and relative hygroscopic-growth factor referenced to the 40% low-RH state.

Comment 11: Line379-380 - "agrees with the CALIPSO version 4": V4 values are prescribed lookup entries, not observations. The manuscript makes this point correctly at Line 447-448; please make the two passages consistent.

Response 11: Thank you for this clarification. We agree that the CALIOP Version 4 lidar ratios cited here are prescribed, subtype-dependent values used in the retrieval algorithm rather than independent observations. We have therefore revised the text to avoid implying observational agreement or validation. Specifically, we now state only that the retrieved $LR_{532}>LR_{1064}$ ordering is qualitatively consistent with the prescribed spectral ordering for several CALIOP V4 aerosol subtypes. We further clarify that these values are used solely as contextual references.

Comment 12: Submitted as a Technical Note but running to ~23 pages with 12 figures. Please either condense (moving the regime analysis to supplementary material) or reclassify as a research article and expand the validation.

Response 12: We have retained the Technical Note format and substantially condensed the main manuscript. The former aerosol-regime analysis (Sect. 3.4 and associated figures) has been moved to the Supplement, together with the detailed reviewer-requested sensitivity analyses. The main text now focuses on the three-stage retrieval framework, the principal retrieval evaluation and optical products, and the RH-dependent conversion to ambient-equivalent lidar-relevant quantities.

Comment 13: A short paragraph on recommended use - which products serve as lidar priors, under what conditions, with what uncertainty would materially increase impact.

Response 13: We have added a short Discussion paragraph defining the intended use of the retrieved products. The multi-wavelength lidar ratios are presented as candidate near-surface lidar-relevant constraints, and may be used as lower-boundary-layer priors only when vertical representativeness is independently supported. They are not intended as universal or vertically resolved lidar ratios. The revised text also distinguishes MC-propagated measurement-input uncertainty from deterministic structural sensitivity and fixed/model-form limitations relevant to the use of these products.

References

Di Antonio, L., Di Biagio, C., Formenti, P., Gratien, A., Michoud, V., Cantrell, C., Bauville, A., Bergé, A., Cazaunau, M., Chevaillier, S., Cirtog, M., Coll, P., D'Anna, B., de Brito, J. F., De Haan, D. O., Dignum, J. R., Deshmukh, S., Favez, O., Flaud, P.-M., Gaimoz, C., Hawkins, L. N., Kammer, J., Language, B., Maisonneuve, F., Močnik, G., Perraudin, E., Petit, J.-E., Acharja, P., Poulain, L., Pouyes, P., Pronovost, E. D., Riffault, V., Roundtree, K. I., Shahin, M., Siour, G., Villenave, E., Zapf, P., Foret, G., Doussin, J.-F., and Beekmann, M.: Aerosol spectral optical properties in the Paris urban area and its

peri-urban and forested surroundings during summer 2022 from ACROSS surface observations, Atmos. Chem. Phys., 25, 3161–3189, https://doi.org/10.5194/acp-25-3161-2025, 2025.

Gialitaki, A., Tsekeri, A., Amiridis, V., Ceolato, R., Paulien, L., Kampouri, A., Gkikas, A., Solomos, S., Marinou, E., Haarig, M., Baars, H., Ansmann, A., Lapyonok, T., Lopatin, A., Dubovik, O., Groß, S., Wirth, M., Tsichla, M., Tsikoudi, I., and Balis, D.: Is the near-spherical shape the "new black" for smoke?, Atmos. Chem. Phys., 20, 14005–14021, https://doi.org/10.5194/acp-20-14005-2020, 2020.

Gluščić, V., Čačković, M., Pehnec, G., and Bešlić, I.: Ionic composition of PM2.5 particle fraction at a coastal urban background site in Croatia, Atmos. Pollut. Res., 11, 2202–2214, https://doi.org/10.1016/j.apr.2020.07.004, 2020.

Haarig, M., Ansmann, A., Baars, H., Jimenez, C., Veselovskii, I., Engelmann, R., and Althausen, D.: Depolarization and lidar ratios at 355, 532, and 1064 nm and microphysical properties of aged tropospheric and stratospheric Canadian wildfire smoke, Atmos. Chem. Phys., 18, 11847–11861, https://doi.org/10.5194/acp-18-11847-2018, 2018.

Heim, M., Mullins, B. J., Umhauer, H., and Kasper, G.: Performance evaluation of three optical particle counters with an efficient “multimodal” calibration method, J. Aerosol Sci., 39, 1019–1031, https://doi.org/10.1016/j.jaerosci.2008.07.006, 2008.

Huang, Y., Kok, J. F., Saito, M., and Muñoz, O.: Single-scattering properties of ellipsoidal dust aerosols constrained by measured dust shape distributions, Atmos. Chem. Phys., 23, 2557–2577, https://doi.org/10.5194/acp-23-2557-2023, 2023.

Lill, E., Costa, E. J., Barry, K., Mirrielees, J. A., Mashkevich, M., Wu, J., Holen, A. L., Cesler-Maloney, M., DeMott, P. J., Perkins, R., Hill, T., Sullivan, A., Levin, E., Simpson, W. R., Mao, J., Temime-Roussel, B., D'Anna, B., Law, K. S., Ault, A. P., Schmitt, C., Pratt, K. A., Fischer, E. V., and Creamean, J.: The abundance and sources of ice nucleating particles within Alaskan ice fog, J. Geophys. Res.-Atmos., 129, e2024JD041170, https://doi.org/10.1029/2024JD041170, 2024.

Liu, L. and Mishchenko, M. I.: Spectrally dependent linear depolarization and lidar ratios for nonspherical smoke aerosols, J. Quant. Spectrosc. Radiat. Transfer, 248, 106953, https://doi.org/10.1016/j.jqsrt.2020.106953, 2020.

Qin, Z., Wang, H., He, A., Sun, Y., Li, J., Zhang, Y., and Zhang, Q.: Backscattering linear depolarization ratio of smoke aerosols from biomass burning, J. Geophys. Res.-Atmos., 129, e2024JD041276, https://doi.org/10.1029/2024JD041276, 2024.

Sinyuk, A., Holben, B. N., Eck, T. F., Giles, D. M., Slutsker, I., Korkin, S., Schafer, J. S., Smirnov, A., Sorokin, M., and Lyapustin, A.: The AERONET Version 3 aerosol retrieval algorithm, associated uncertainties and comparisons to Version 2, Atmos. Meas. Tech., 13, 3375–3411, https://doi.org/10.5194/amt-13-3375-2020, 2020.

Turšič, J., Podkrajšek, B., Grgić, I., Ctyroky, P., Berner, A., Dusek, U., and Hitzenberger, R.: Chemical composition and hygroscopic properties of size-segregated aerosol particles collected at the Adriatic coast of Slovenia, Chemosphere, 63, 1193–1202, https://doi.org/10.1016/j.chemosphere.2005.08.040, 2006.

Wang, L., Bervida Mačak, M., Stanič, S., Bergant, K., Gregorič, A., Drinovec, L., Močnik, G., Yin, Z., Yi, Y., Müller, D., and Wang, X.: Investigation of aerosol types and vertical distributions using

polarization Raman lidar over Vipava Valley, Remote Sens., 14, 3482, https://doi.org/10.3390/rs14143482, 2022.

Wang, L., Stanič, S., Bergant, K., Eichinger, W., Močnik, G., Drinovec, L., Vaupotič, J., Miler, M., Gosar, M., and Gregorič, A.: Retrieval of vertical mass concentration distributions – Vipava Valley case study, Remote Sens., 11, 106, https://doi.org/10.3390/rs11020106, 2019.

Yus-Díez, J., Drinovec, L., Alados-Arboledas, L., Titos, G., Bazo, E., Casans, A., Patrón, D., Querol, X., Gonzalez-Romero, A., Perez García-Pando, C., and Močnik, G.: Characterization of filter photometer artifacts in soot and dust measurements – laboratory and ambient experiments using a traceably calibrated aerosol absorption reference, Atmos. Meas. Tech., 18, 3073–3093, https://doi.org/10.5194/amt-18-3073-2025, 2025.

Zinke, J., Nilsson, E. D., Markuszewski, P., Zieger, P., Mårtensson, E. M., Rutgersson, A., Nilsson, E., and Salter, M. E.: Sea spray emissions from the Baltic Sea: comparison of aerosol eddy covariance fluxes and chamber-simulated sea spray emissions, Atmos. Chem. Phys., 24, 1895–1918, https://doi.org/10.5194/acp-24-1895-2024, 2024.

Response to the Referee 2's Comments

October 05, 2026

Accurate characterization of key aerosol optical properties—such as the complex refractive index (CRI), single scattering albedo (SSA), and lidar ratio (LR)—is paramount for assessing aerosol radiative impacts. However, observational constraints and limitations in retrieval theories introduce substantial uncertainties, making precise radiative evaluations a persistent challenge. To address this issue, the authors present a clear retrieval framework based on field observations collected in Slovenia in April 2016 (including SMPS–OPC size distributions, AE33-derived absorption coefficients, and ambient relative humidity data). Using this approach, they successfully derive dry-state homogeneous-equivalent CRIs alongside RH-corrected, lidar-relevant SSAs and LRs across three key wavelengths (355, 532, and 1064 nm). This work provides a viable bridge connecting dry in situ CRI retrievals with ambient, multi-wavelength aerosol optical products relevant for lidar applications. This manuscript presents an interesting approach, but there are several questions that remain to be addressed. My comments are listed as follows:

Response: We thank the reviewer for the time and effort, which have made a significant contribution to the improvement of the paper.

Major Comments:

Comment 1: The practical utility of the proposed retrieval framework requires further elaboration. In the Discussion section, the manuscript notes that "because the framework is constrained by near-surface in situ observations, its products are most directly applicable as local lidar constraints for near-surface or well-mixed lower-boundary-layer conditions, rather than as direct representations of the full vertically resolved aerosol column." Given that the retrieved aerosol optical parameters are primarily representative of near-surface conditions, could the authors clarify how this framework meaningfully advances the evaluation of aerosol radiative effects? Since radiative forcing assessments generally require column-integrated or vertically resolved profile data, near-surface results alone appear insufficient for this purpose. For example, a key purpose of determining the lidar ratio is to constrain lidar inversions when retrieving extinction coefficient profiles. However, since the current framework yields only near-surface lidar ratios, these values are not readily applicable to solving vertical extinction coefficient profiles.

Response 1: We thank the reviewer for this important comment. We agree that the spatial representativeness of the retrieved optical properties must be distinguished from their potential role in lidar and radiative applications. The present framework directly derives aerosol optical properties constrained by near-surface in situ observations; it does not independently retrieve a vertically resolved aerosol profile.

Importantly, however, this does not restrict the retrieved quantities to purely point-level interpretation. Ground-based optical constraints can contribute to vertically resolved lidar retrievals when they are combined with independent information on the vertical atmospheric structure. For example, Liu et al. (2024) used ground-based particle-size and composition measurements together with vertically resolved meteorological information to estimate boundary-layer aerosol optical profiles and showed that representative lidar ratios can be obtained from surface observations under sufficiently well-mixed boundary-layer conditions.

Beyond this conditional role in lower-boundary-layer lidar retrievals, a complementary future application is the evaluation of aerosol-type-dependent LR priors. For example, Miffre et al. (2026) developed a laboratory method combining 180° backscatter and cavity ring-down extinction measurements to determine the LR of controlled aerosol samples and to evaluate light-scattering models. Such laboratory measurements could complement ambient, multiwavelength estimates from the present framework.

Accordingly, the LR retrieved in the present study is interpreted first as a local, aerosol-state-dependent constraint on the lidar ratio. It can be used to evaluate the physical plausibility of an assumed LR at the surface and, when independent observations establish sufficient vertical representativeness, can provide an additional constraint for lower-boundary-layer lidar retrievals. The present study does not perform this vertical coupling because suitable collocated vertically resolved observations are not available for an independent evaluation of that step.

The radiative relevance is analogous. The retrieved CRI, SSA, and associated optical properties constrain the local aerosol optical state required by radiative-transfer calculations, whereas column radiative-effect estimates additionally require independent information on the vertical or column aerosol distribution. We have revised the manuscript to distinguish clearly between the direct local products of the framework and their conditional use as constraints in vertically resolved lidar or radiative applications.

Comment 2: Limitations of Data Timeliness and Sample Size: The main conclusions of this manuscript appear to be constrained by significant data limitations. First, using decade-old observations raises questions regarding data timeliness and present-day relevance. Second, a dataset spanning merely ten days represents a severely restricted temporal sample. It remains doubtful whether such a brief snapshot is statistically sufficient to yield generalizable or robust atmospheric insights. The authors must clarify how a ten-day regional dataset can support broader, universal claims, or reframe the study's scope to

reflect its site-specific and short-term nature.

Response 2: We thank the reviewer for raising this important issue. We agree that the temporal scope of the April 2016 Vipava observations limits their use for characterizing long-term or present-day aerosol conditions at the site. We have therefore clarified the scope of the manuscript. The primary contribution of this Technical Note is methodological: the field observations are used to develop and evaluate the decoupled retrieval framework under real mixed-aerosol conditions, rather than to establish an aerosol climatology for the Vipava Valley.

The field campaign covered 7–23 April 2016, although the effective retrieval coverage was reduced by instrument availability, synchronization requirements, and quality-control screening. The retained observations allow the framework to be evaluated across the range of mixed-aerosol conditions encountered during the campaign, including its internal consistency, sensitivity, and aerosol-state-dependent optical response. They are not, however, interpreted as evidence for climatological frequencies, long-term site statistics, or universal aerosol optical relationships.

Accordingly, we have revised the manuscript to distinguish the methodological contribution of the framework from the temporal and regional representativeness of this particular field application. Campaign-derived CRI, SSA, LR, RH responses, and regime-dependent differences are now explicitly interpreted in the context of the aerosol states sampled during the Vipava campaign. The age of the observations therefore limits the present-day environmental representativeness of these results, but does not preclude their use as a field-based demonstration of the retrieval framework. Broader applicability of the framework across aerosol environments requires evaluation with additional datasets from other sites and periods.

Specific Comments:

Comment 1: Sample Size Considerations in Figure 5: Regarding the boxplots presented in Figure 5, are the sample sizes (*N*) for each individual box roughly comparable? A substantial disparity in sample sizes could skew the statistical distribution and potentially alter the derived conclusions. To ensure statistical rigor and transparency, the authors should explicitly specify the sample count for each box, either annotated directly within the figure or detailed in the caption.

Response 1: Thank you for this helpful suggestion. We have revised the caption of Figure 5 to report the sample counts explicitly for each boxplot group. We also clarified that the compared cases were evaluated on the same post-QC cohort, so the boxplots within each comparison are based on directly comparable sample sets. This revision improves the transparency of the statistical basis of the distributions and helps the reader assess whether differences among boxplots may be influenced by unequal group sizes.

Comment 2: Figure Sizing and Format Consistency: The dimensions of figures throughout the manuscript should be kept as uniform as possible to ensure ease of reading. Several figures appear overly small (e.g., Figure 10). The authors are advised to adjust figure scales for better visual clarity.

Response 2: Thank you for this suggestion. We re-exported the main-text and supplementary figures using harmonized panel widths, font sizes, axis-label sizes, line widths, marker sizes, and spacing. The detailed regime-resolved analysis formerly associated with Sect. 3.4 was moved to Supplement Sect. S7, where the figures were enlarged and reformatted for improved legibility; the main text retains a concise summary and explicit cross-references.

Comment 3: Marker Visibility in Figure 10: Specifically in Figure 10, the data points/markers are too small to be visually distinguished. Please increase the marker size to improve legibility.

Response 3: Thank you for this helpful suggestion. We condensed Sect. 3.4 and moved the detailed regime-resolved analysis and associated figures to Supplement Sect. S7 (Figs. S6–S10).

We have revised the figure to improve visual readability by increasing marker sizes and enhancing the distinction among different FVF groups. In the revised figure, the three FVF categories are represented using larger and distinct markers, and the corresponding sample numbers are explicitly provided in the legend. We have also added the corresponding AAE values for each FVF group to provide additional context for the absorption-related differences associated with the observed LR spectral variations.

Comment 4: Physical Interpretation of Figure 12c: In Figure 12c, the results indicate that the influence of relative humidity (RH) becomes more pronounced at longer wavelengths. What is the physical mechanism behind this wavelength dependence? Furthermore, why does the behavior at 1064 nm run counter to the trends observed at 355 nm and 532 nm? Further clarification on these optical/hygroscopic mechanisms is needed.

Response 4: Thank you for this comment. The former Figure 12c is now presented as Figure 8c, while the corresponding extinction–backscatter decomposition is shown in Figure 9.

The results show that the RH effect should not be interpreted as increasing monotonically toward longer wavelengths. Hygroscopic water uptake changes both particle size and the effective complex refractive index, and both changes affect extinction and 180° backscatter through the size- and wavelength-dependent Mie response. The particle-size increase shifts the aerosol population across wavelength-dependent Mie size-parameter regimes, while the accompanying refractive-index dilution modifies the scattering and absorption efficiencies. Because 180° backscatter is additionally sensitive to the angular-scattering response, its relative change need not follow that of extinction. Because $LR = \alpha_{ext} / \beta_{back}$, the sign of the LR response

depends on the relative changes in extinction and backscatter.

At 355 and 532 nm, the median relative enhancement of extinction exceeded that of backscatter, consistent with positive median paired LR changes of +1.91% and +4.15%, respectively. At 1064 nm, this relationship reversed: the relative enhancement of backscatter exceeded that of extinction, with a median paired LR change of −4.20%. Thus, the opposite 1064-nm response results from the reversal in the relative extinction–backscatter enhancement, rather than from a monotonic strengthening of the RH effect toward longer wavelengths. The extinction–backscatter decomposition is shown in Fig. R1 and has been incorporated as Fig. 9 in the revised manuscript.

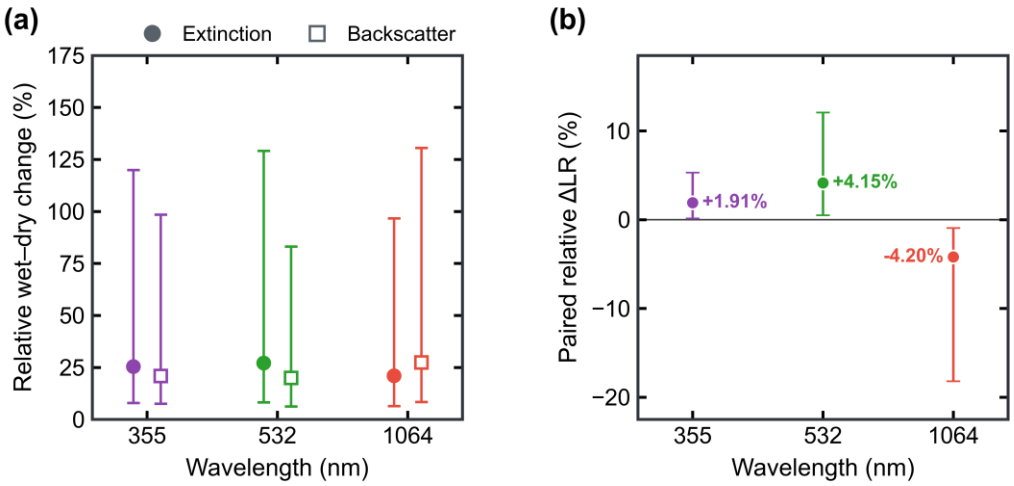

Figure R1. Wavelength-dependent RH effects on aerosol optical properties. (a) Median relative wet-reference changes in extinction and 180° backscatter at 355, 532, and 1064 nm. (b) Median hourly paired wet-versus-reference relative changes in lidar ratio. Markers denote medians and error bars denote interquartile ranges for the 275 RH-active hours from the final 304-hour post-QC cohort. At 1064 nm, lidar ratio decreased in 239 of 275 hours. The same analysis is presented in Fig. 9 of the revised manuscript.

Comment 5: Justification of Literature Comparison in Table 2: In the Discussion, the authors compare their results with previous literature in Table 2. However, the rationale and added value of this comparison require further clarification. Reported lidar ratios (LR) across different studies vary widely depending on retrieval methodologies, observation sites, and spatial representativeness (e.g., the near-surface nature of this study vs. column measurements). In addition, LR is highly sensitive to aerosol type, a factor that is not comprehensively categorized or stratified in this work. Given these fundamental discrepancies, what specific insights does Table 2 offer, and how does it advance the discussion?

Response 5: Thank you for this important comment. Note that the former Table 2 is now Table

3 in the revised manuscript. In the revised manuscript, we have clarified that Table 3 is intended as a contextual comparison rather than an external validation dataset. The purpose of this comparison is not to demonstrate one-to-one agreement with previous LR retrievals, but to place the retrieved wavelength-dependent LR behaviour within the range of reported multi-wavelength LR behaviours under different observational contexts and to highlight the limited availability of 1064-nm LR information.

We have further revised the discussion to emphasize that the studies included in Table 3 represent different observational conditions, including ground-based lidar observations, vertically resolved aerosol-layer measurements, and operational lidar retrieval schemes. Therefore, aerosol classifications reported in these studies are retained only to describe their original measurement contexts and are not interpreted as direct aerosol-type equivalents of the Vipava Valley aerosol population.

The revised discussion now focuses on wavelength-dependent tendencies rather than absolute LR agreement. Specifically, previous studies showing both increasing and decreasing LR trends with wavelength demonstrate that LR spectral behaviour is not universal, but depends on coupled effects of aerosol microphysical state and observational constraints. This comparison therefore supports the motivation for deriving locally constrained, physically based LR estimates rather than applying fixed empirical LR assumptions across different aerosol environments.

References

Liu, X., Alves Gouveia, D., Henzing, B., Apituley, A., Hensen, A., van Dinther, D., Huang, R., and Dusek, U.: Aerosol optical properties within the atmospheric boundary layer predicted from ground-based observations compared to Raman lidar retrievals during RITA-2021, Atmos. Chem. Phys., 24, 9597–9614, https://doi.org/10.5194/acp-24-9597-2024, 2024.

Miffre, A., Pacoret-Berenger, C., Genoud, A. P., and Rairoux, P.: A novel laboratory methodology to evaluate the particle extinction-to-backscatter ratio or particle lidar ratio of aerosols, Sci. Rep., 16, 28738, https://doi.org/10.1038/s41598-026-61997-3, 2026.